Heterogeneous Catalysis Hot Paper

How to cite: *Angew. Chem. Int. Ed.* **2021**, *60*, 17522–17530
International Edition: doi.org/10.1002/anie.202102106
German Edition: doi.org/10.1002/ange.202102106

Precise Identification and Characterization of Catalytically Active Sites on the Surface of γ-Alumina**

Konstantin Khivantsev[+], Nicholas R. Jaegers[+], Ja-Hun Kwak[+],* Janos Szanyi,* and Libor Kovarik[+]**

Abstract: *γ-alumina is one of the oldest and most important commercial catalytic materials with high surface area and stability. These attributes enabled its use as the first commercial large-scale heterogeneous catalyst for ethanol dehydration. Despite progress in materials characterization the nature of the specific sites on the surface of γ-alumina that are responsible for its unique catalytic properties has remained obscure and controversial. By using combined infrared spectroscopy, electron microscopy and solid-state nuclear magnetic resonance measurements we identify the octahedral, amphoteric $(O)_5Al(VI)$-OH sites on the (100) segments of massively restructured (110) facets on typical rhombus-platelet γ-alumina as well as the (100) segments of irrational surfaces (invariably always present in all γ-alumina samples) responsible for its unique catalytic activity. Such $(O)_5Al(VI)$-OH sites are also present on the macroscopically defined (100) facets of γ-alumina with elongated/rod-like geometry. The mechanism by which these sites lose -OH groups upon thermal dehydroxylation resulting in coordinatively unsaturated penta-coordinate $Al^{+3}O_5$ sites is clarified. These coordinatively unsaturated penta-coordinate Al sites produce well-defined thermally stable Al-carbonyl complexes. Our findings contribute to the understanding of the nature of coordinatively unsaturated Al sites on the surface of γ-alumina and their role as catalytically active sites.*

Introduction

Since Vladimir Ipatieff's discovery in 1902 that γ-alumina can be used as a robust large-scale catalyst for ethanol dehydration to produce ethylene,[1,2] this material has emerged as the oldest and most commercially important heterogeneous catalysts, featuring high surface area and excellent high-temperature stability.[3] Subsequently, γ-alumina found wide applications as a support for organometallic molecular complexes, isolated ions, nanoparticles, etc.,[1] the latter becoming industrially relevant for automotive applications and petroleum refining.[4–6] The precise nature of the catalytically active surface sites of γ-alumina remains obscure despite a multitude of studies aimed at clarifying this uncertainty.[7–12] The origin of this challenge lies in the complex crystalline structure of γ-alumina which is still unresolved, and which evolves into the closely related delta- and theta- transitional aluminas with thermal treatments above 850 °C. This gap in the knowledge prevented full molecular understanding of the surface of γ-Al_2O_3.[7–11] Only recently, with the aid of state-of-the-art high-angle annular dark field scanning transmission electron microscopy (HADDF-STEM) and high resolution (HR) TEM imaging coupled with the diffraction and solid-state nuclear magnetic resonance (NMR) methods, Kovarik and co-workers solved the structures of delta- and theta- transition alumina phases.[7–13] In contrast to previous understanding, it was revealed that the δ-structure is an interwoven intergrowth in two dime3nsions of crystallographically distinct $\delta_{1,2,3,4}$ phases.[8–11] By correlating the imaging and spectroscopy results with density functional theory (DFT) calculations, θ-Al_2O_3 was found to be a highly defective structure, which can be interpreted as a structure consistent with β-Ga_2O_3 phase containing a high density of δ_3-Al2O3-like defects that significantly modify the bonding environment.[9] In prior studies, θ-Al_2O_3 was considered isostructural to β-Ga_2O_3. Despite these advances in molecular understanding of the structures and surfaces of θ- and δ-Al_2O_3, the bulk structure of γ-alumina remains unknown.[12,13] Numerous studies have aimed at understanding γ-alumina using infrared spectroscopy, NMR, and DFT calculations, and specifying the active sites on the surface of γ-alumina that are responsible for both catalysis and the anchoring of metal atoms/organometallic fragments/nanoparticles.[14–22] In those studies,[14–20] tri-coordinate sites were suggested to form on the dehydroxylated alumina surfaces upon heating to 400 °C and were probed with the IR spectrum of adsorbed nitrogen.[14–20] However, the theoretical parts of these studies included several critical assumptions regarding surface terminations, their reconstruction and most importantly crystal structure of γ-alumina. For

[*] Dr. K. Khivantsev,[+] Dr. N. R. Jaegers,[+] Dr. J. Szanyi, Dr. L. Kovarik[+]
Institute for Integrated Catalysis
Pacific Northwest National Laboratory
Richland, WA 99352 (USA)
E-mail: Konstantin.Khivantsev@pnnl.gov
Janos.Szanyi@pnnl.gov
Libor.Kovarik@pnnl.gov
Prof. J.-H. Kwak[+]
Ulsan National Institute of Science and Technology (UNIST)
Ulsan, 44919 (Republic of Korea)
E-mail: jhkwak@unist.ac.kr
[+] These authors contributed equally to this work.

[**] A previous version of this manuscript has been deposited on a preprint server (https://doi.org/10.26434/chemrxiv.11829576.v1).
Supporting information and the ORCID identification number(s) for the author(s) of this article can be found under: https://doi.org/10.1002/anie.202102106.

example, the assumption regarding the crystallographic structure of γ-alumina as defective spinel containing the ratio between tetra- and octahedral Al atoms in the bulk structure as 25% and 75%, explicitly stated in multiple studies,[14–20] naturally raises concern for their validity.[12,13] To assess these concerns, high-field solid-sate NMR was employed to observe the aluminum distributions in two different γ -alumina samples with a rhombus-platelet geometry (surface area 70 $m^2 g^{-1}$, synthesized in-house and 200 $m^2 g^{-1}$ surface area commercial SBA-200 of nanosized platelet-type morphology). XRD of both samples and HAADF-STEM/HRTEM images (with the corresponding discussion) are shown in Figure S1 and S2. The rhombus-platelet sample exhibits a ≈63–35% while the SBA-200 $m^2 g^{-1}$ possesses ≈68–30% octa-:tetrahedral Al^{3+} ratio (Figure 1C, S3). These values are indicative of a bulk crystal structure very different from the models assumed in prior reported literature, rendering them poorly representative of the -OH groups on the surface and of surface-adsorbate interactions. It is important to note that most infra-red -OH group assignments on the surface of γ-alumina come from DFT models[14–20,22] and intuition,[21] however definitive proof in the assignments is lacking. It

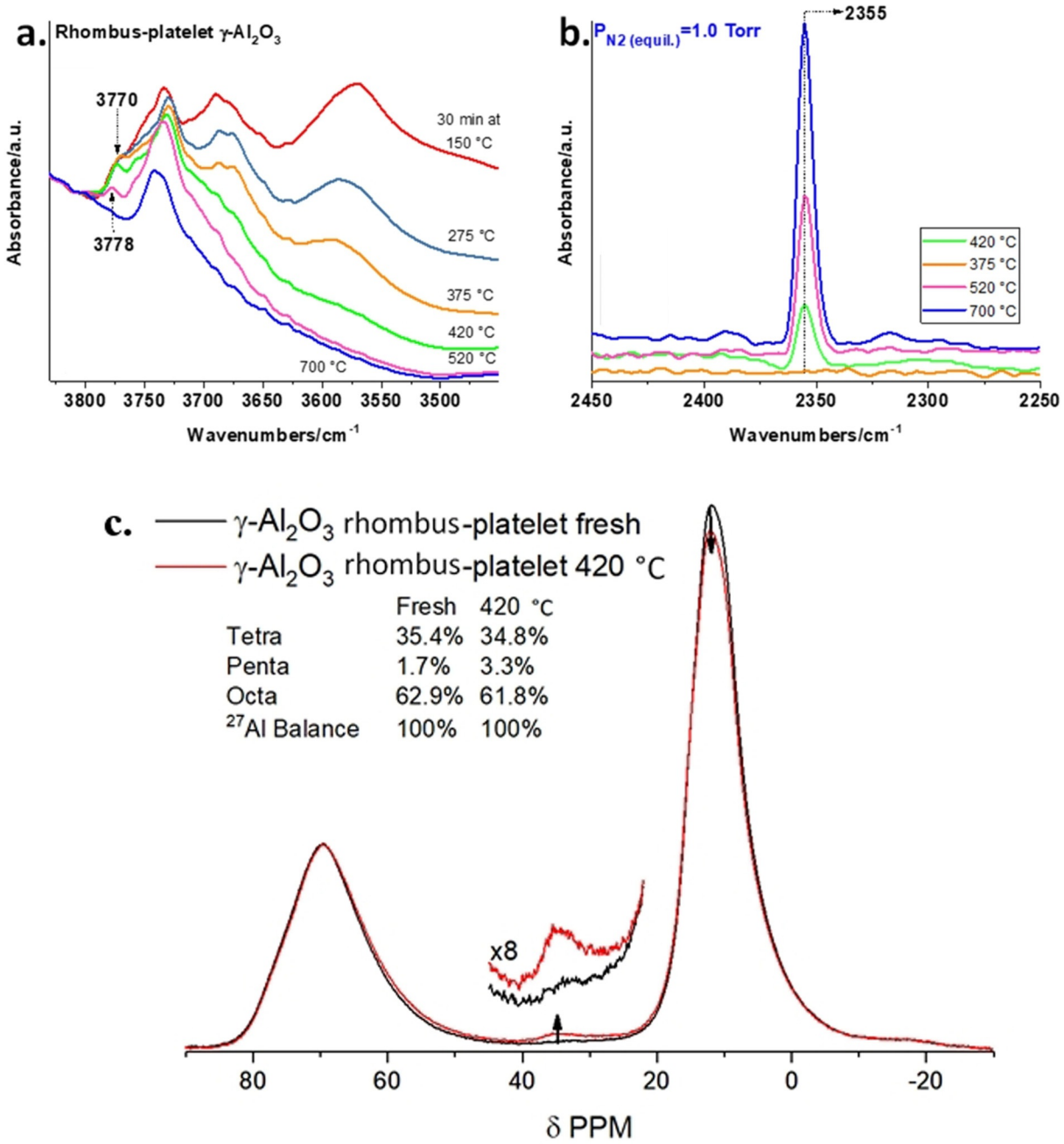

Figure 1. a) In situ FTIR during heating of the rhombus-platelet γ-alumina pellet under vacuum (30 min at ≈10^{-7} torr) after cooling back to 25 °C; spectra were recorded on the same tablet. b) FTIR during 5 N_2 torr N_2 adsorption (equilibrium pressure 1.0 torr) at 25 °C on γ-alumina treated at different temperatures after each temperature treatment. c) Solid-state high-field ^{27}Al NMR data for rhombus-platelet γ-alumina before and after prolonged heating at 420 °C (inset shows 8 times magnified peak between 40 and 20 ppm belonging to penta-Al sites).

was previously shown that penta-coordinate sites exist on the γ-alumina surface and are the anchoring points for isolated Pt atoms, PtOx rafts as well as tungsten oxide species responsible for creating catalytically active structure.[23] Penta-coordinate Al^{3+} sites in the Pt anchoring study were suggested to form on the (100) facet of the surface upon dehydration/dehydroxylation.[23] It is noted that the DFT surface model used in that study was not representative of the real surface; furthermore, SBA-200 material (Figure S2 c–f) was used with a mixture of nanosized (100) and (111) facets on nanoplatelets as well as less defined crystals (Figure S2 c,e). It was further suggested that the 5-coordinate Al^{3+} sites on macroscopically defined (001) facets are responsible for ethanol dehydration activity of γ-alumina.[24,25] However, for typical rhombus-platelet and SBA-200 alumina samples, no macroscopically defined (100) facets can be found yet they still show catalytic activity for ethanol dehydration (Figure S2, S4 and S5).

Herein, the -OH band at ≈3770-3780 cm^{-1} in the IR spectrum is identified as the amphoteric Al^{VI}-OH site on the heavily restructured (110) facets of rhombus-platelet γ-alumina, responsible for its catalytic activity in alcohol dehydration. These -OH groups serve as the precursor to coordinatively unsaturated penta-coordinate Al^{V} sites.

Zubkov and co-workers demonstrated in the 1980s[26] that γ-alumina was able to form a dinitrogen complex with molecular nitrogen after thermal dehydration, exhibiting the N-N stretching band at 2360 cm^{-1}. Coperet et al., later stated that N_2 is a selective probe for 3-coordinate Al^{3+} sites that form upon dehydroxylation of the tetrahedral O_3-Al^{IV}-OH sites on the (110) facet, which coincides with the formation of a band at 2355 cm^{-1}. It was later suggested that such tri-coordinate Al^{3+} ions anchored organometallic fragments and produced active catalysts while organometallic fragments anchored on other Al^{3+} sites did not produce active catalysts.[15,16,18] However, these studies suffered from inaccurate structural representation in the models employed, casting doubt on the conclusions drawn.[10,12,13] Furthermore, a correlation between the observed -OH groups and the ability to activate dinitrogen, which we provide in our study, was absent. Figure S6 confirms that heated γ-alumina is indeed able to coordinate dinitrogen.

Results and Discussion

Both the OH- and N-N stretching vibrations of rhombus-platelet γ-alumina upon thermal treatment were studied with FTIR. The sample was pressed into a thin pellet and IR studies were conducted in the transmission mode. After dehydrating in vacuum and cooling to 25 °C ($< 10^{-7}$ torr for 30 minutes at each temperature), FTIR spectra were collected. Upon cooling to 25 °C adsorption of N_2 was performed (at $P_{equil} = 1$ torr) (panels **a** and **b** of Figure 1).

As the annealing temperature increases the intensities of all -OH groups begin to decline except the one centered at ≈3770–3780 cm^{-1}. This indicates dehydration (and/or dehydroxylation) is taking place on the surface at elevated temperatures. The 3770 cm^{-1} band starts to decrease when the temperature exceeds 375 °C, and it fully disappears after annealing at 700 °C. Simultaneously, the adsorption of dinitrogen at an equilibrium pressure of ≈1 torr was carried out at room temperature after each thermal treatment. Notably, no N_2 adsorption, characterized by the IR stretching vibrational feature at 2355 cm^{-1}, takes place after annealing at 375 °C, despite the decline of all -OH bands, except the one centered at 3770 cm^{-1}. When the annealing temperature exceeds 420 °C, the intensity of the ≈3770–3780 cm^{-1} band starts to decrease and N_2 adsorption occurs (Figure 2). This indicates, that only when the ≈3770 cm^{-1} band starts to decrease a new Al^{3+} site (free of -OH group) evolves which is capable of adsorbing N_2. From 420 to 700 °C the intensity of the sharp N-N band in the FTIR spectra increases. Table S1

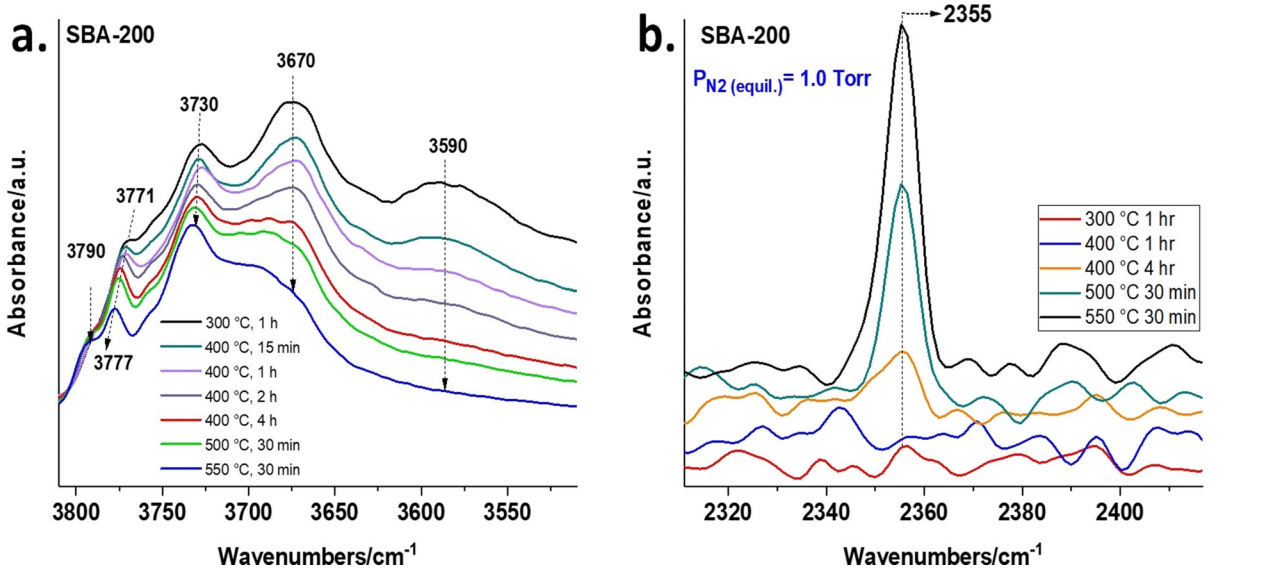

Figure 2. a) In-situ FTIR during SBA-200 heating under vacuum (spectra recorded after pre-treating at each temperature at a specified time and then cooling back down to 25 °C). b) FTIR during 5 N_2 torr N_2 adsorption (equilibrium pressure 1.0 torr) at 25 °C on γ-alumina after annealing treatments shown in Figure 2 a).

illustrates the correlation between the N-N band formation and the intensity decrease of the 3770 cm^{-1} -OH vibrational feature, confirming that adsorption of N_2 takes place on the Al^{3+} sites that form upon dehydroxylation of a specific type -OH groups.

It is noted that as the temperature increases from 375 to 520 °C the -OH group visible at 3771 cm^{-1} shifts to 3778 cm^{-1}. Elimination of dipole-dipole coupling interactions is expected to shift the spectrum in the opposite direction, negating this as a possible explanation. Therefore, the presence of a family of similar Al-OH sites with slightly varying properties (i.e., second-shell ligand environment) is responsible for this effect: more specifically, Al-OH groups at slightly higher frequencies are the most thermally stable ones (the last ones to lose their -OH groups).

Quantitatively similar findings are observed for the SBA-200 sample (Figure 2).

Two different modes of dehydration/dehydroxylation may be active on this surface:

$$\text{Al-OH} + \text{Al-OH} \rightarrow \text{Al-O-Al} + H_2O. \quad (1)$$

In this case, no change in Al^{3+} coordination is expected; however, the data indicate that Al coordination decreases since this Al atom without OH group activates N_2. Therefore, the entire -OH group must be lost. The following process can explain the loss of -OH to form an undercoordinated Al^{3+} site:

$$\text{Al-OH} + H^+ \rightarrow Al_{\text{undercoordinated}} + H_2O. \quad (2)$$

Brønsted acidic -OH groups of bridging Al-OH-Al sites (Al-OH-Al ≈3660–3680 cm^{-1}) harbor mobile protons which may interact with the basic -OH groups (≈3770–3780 cm^{-1}) and desorb as water. Since the intensities of the 3770 and 3660 cm^{-1} bands decrease in concert (Figure 1a, Figure 2a), the 3770 cm^{-1} band may be assigned to a basic (amphoteric) Al-OH site. Its basicity is confirmed by the observation of the formation of bicarbonate via interaction with carbon dioxide. CO_2 (which is acidic) interacts only with -OH groups possessing basic character resulting in the formation of a bicarbonate. Figure S7 illustrates that the Al-OH band represented by the ≈3770 cm^{-1} feature selectively reacts with CO_2 to form bicarbonates. (The C-O stretching region is complex due to multiple modes of CO_2 interaction with the surface, but the 3606 cm^{-1} band unambiguously demonstrates the formation of bicarbonates that form at the expense of the OH group with basic character represented by the IR band at 3770 cm^{-1}.)

The ligand environment of the Al-OH site responsible for the ≈3770 cm^{-1} IR feature can be either octa-, penta- or tetrahedral. Dehydroxylation of that site would then produce undercoordinated Al^{3+} ions maintaining an Al valency of +3: $Al^{V}O_5$ (penta-), $Al^{IV}O_4$ (tetra-) and $Al^{III}O_3$ (tri-coordinate), respectively. High field solid-state ^{27}Al NMR is extremely useful[27,28] to illuminate the changes in surface coordination during the annealing process and it confirms that the ≈3770–3780 cm^{-1} IR band represents the -OH group of the amphoteric O_5Al^{VI}-OH site. Only three types of Al^{3+} sites are observed from the beginning until the end of dehydroxylation in Figure 1C (tetra-, penta- and octahedral), in agreement with previous studies.[23,24] Most importantly, the total Al site balance that can be determined with high precision in our solid-state NMR experiments (we use the same amount of sample in the rotor for experiments before and after dehydration; furthermore, the total Al signal balance agrees in multiple experiments before and after dehydration within 0.2% of the total spectral Al signal area, retains unity after the heat treatment, signifying that no tri-coordinate or other undetectable Al species evolves upon annealing (within the error margin; moreover, if coordinatively unsaturated sites, other than the Al_{penta} sites, indeed evolved during the thermal treatment, FTIR adsorption with CO and N_2 probe molecules (IR with CO probe molecule is more sensitive than NMR due to the very high molar extinction coefficients of metal-carbonyl complexes resulting in very intense C-O stretching bands) would be able to distinguish those as discussed in the manuscript vide infra) (Figure 1C). The number of octahedral Al^{3+} sites decreases at the expense of the evolving penta-coordinate Al^{3+} sites upon heating (Figure 1C).

This indicates that the ≈3770 cm^{-1} band belongs to octahedral O_5Al^{VI}-OH species which produces penta-coordinate O_5Al^{V} sites upon dehydroxylation that, in turn, can bind N_2. It has been suggested in multiple previous studies that the "tri-coordinate" Al^{3+} site on (110) terminated facet,[14–20] is capable of adsorbing nitrogen and that it is also responsible for anchoring organometallic fragments to generate active molecular catalysts.[14–20] Our results indicate that neither of these functions should be ascribed to the tri-coordinate site but instead to the penta O_5Al^{V} site that is formed during dehydroxylation of O_5Al^{VI}-OH. It is important to note that even DFT calculations in the studies that ascribed N_2 binding to tri-coordinate Al^{3+}sites on (110) facets, indicated the very high temperatures required to form tri-coordinate Al_1O_3 sites (on the order of 900 °C), highlighting the unfavourability of their formation in the studied models.

We now show that a main portion of these octahedral O_5Al^{VI}-OH sites is located on macroscopically defined and heavily restructured (110) surfaces (Figure 3). With high-resolution transmission electron microscopy (HRTEM), we were able to visualize the different facets of the rhombus-platelet γ-alumina sample. Analysis of the high resolution images revealed that the formation of O_5Al^{V} sites on the macroscopically defined (110) surfaces was possible due to significant surface reconstructions, which breaks down the surface to (111) and (100) segments (Figure 3a–c). The required symmetry for the terminal OH groups on penta-coordinate sites can be found only on the (100) segments. In our HRTEM observations the (111) segments can be visualized directly because they form ridges that are aligned along the observation direction. The presence of the (100) segments is inferred from the observation that the (111) ridges have finite length on the (110) surface, and end with the (100) termination. The observation shown in Figure 3b depicts a thicker portion of (110) facets with multiple finite length ridges in apparent overlap. A schematic of this geometry is shown in Figure 3a. The higher thermodynamic

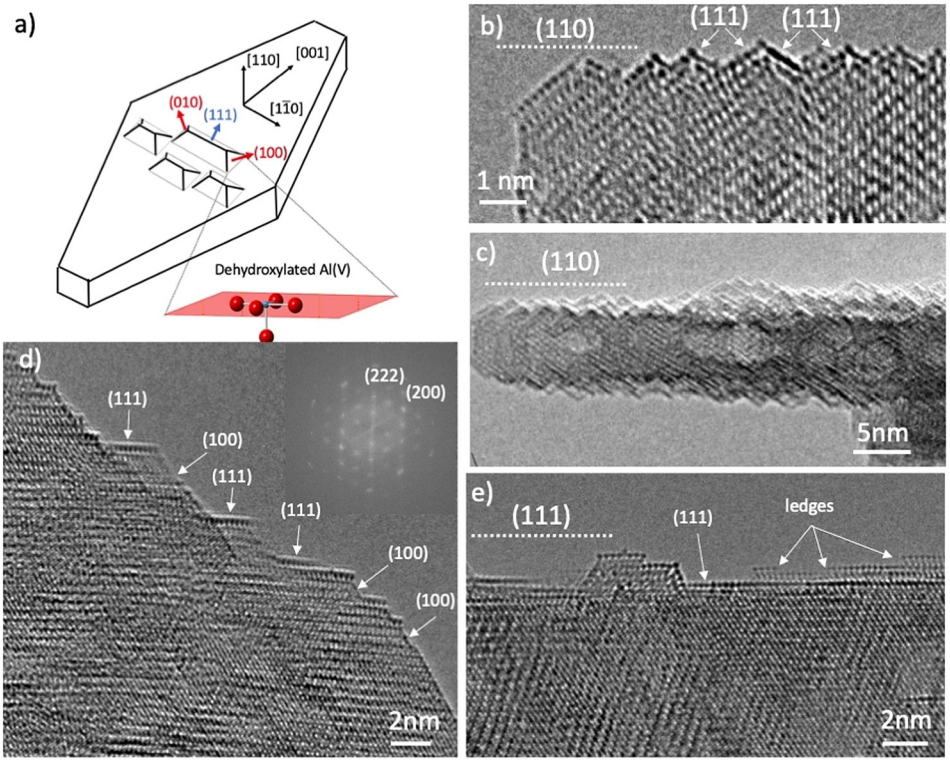

Figure 3. a–c) HRTEM observations of (110) surfaces of rhombus-platelet γ-alumina. The (110) surface undergoes a significant reconstruction and the macroscopically defined surface develops (111) and (100) facets. d) HRTEM observation of an irrational surface of γ-alumina consisting of (100) and (111) segments. e) HRTEM observation of (111) surface facet.

stability of the (111) and (100) facets compared to (110) plays a role in the observed restructuring. The (111) facet does not contain coordinatively unsaturated $Al^{V}O_5$ sites, (Figure 3e, Figure S8).

We also note that all γ-alumina samples contain, in addition to well-defined crystals, less defined crystals with irrational surfaces (Figure 3d, Figure S9, Figure S2e). Those surfaces also break down into (111) and (100) segments with $Al^{V}O_5$ sites present on them from dehydroxylation of Al^{VI}-OH sites represented by the $\approx$3770 cm^{-1} band in the IR spectrum. Depending on the synthesis conditions, their amount varies. The rhombus-platelet particles contain virtually no macroscopically defined (100) facets (due to its geometry), and the Al^{VI}-OH sites are located predominantly on the restructured (110) surfaces (visualized in Figure 2).

We note, that in the IR spectrum of the SBA-200 material a band at 3790 cm^{-1} coexists with the main feature at 3770–3780 cm^{-1} (Figure 2a); this band is practically absent in the IR spectrum of the rhombus-platelet sample (Figure 1a). The same pronounced feature at 3790 cm^{-1} is also seen for the elongated, rod-like alumina sample (Figure S10) which contains a significant fraction of macroscopically defined (100) facets. The Al^{VI}-OH feature at 3790 cm^{-1} is much more resistant to thermal treatment than the 3770 cm^{-1} feature (Figure 2a, Figure S10). As we mentioned earlier, the -OH stretching band at 3770–3780 cm^{-1} contains contributions from very similar, yet subtly different (with slightly varying local environments) Al^{VI}-OH sites; furthermore, the higher the frequency of the Al^{VI}-OH site, the harder it is to remove by dehydroxylation. Thus, the higher thermal stability of the Al^{VI}-OH groups represented by the 3790 cm^{-1} band is not surprising. It is tempting to assign it to the Al^{VI}-OH sites on the macroscopically defined (100) faces, whose fraction is very small (due to the geometry) in the rhombus-platelet sample and increases significantly in the rod-like sample. However, we also note that SBA-200 sample that (in addition to nanoplatelets) contains less defined nanocrystals and irrational surfaces still has this well-pronounced feature (Figure 2a). Therefore, it is very likely that the samples containing irrational surfaces have the additional population of O_5Al^{VI}-OH groups giving rise to the 3790 cm^{-1} feature on those surfaces. The rod-like sample probably contained a higher amount of such irrational surface than the rhombus-platelet sample due to synthesis conditions.

It is also important to note that SBA-200 is in contact with air when loaded in the IR cell and presents no $\approx$3790–3770 cm^{-1} bands. These -OH bands appear only after heating above 250 °C under vacuum in the IR cell. Their appearance is due to the desorption of carbon dioxide which interacts with the basic (amphoteric) -OH groups and prevents their observation (Figure S11). This observation accounts for the lower activity of the 200 °C calcined alumina relative to the 500 °C calcined alumina for ethanol dehydration.[26] (We recommend that all alumina samples be pre-treated at least at $\approx$300 °C in flowing air prior to measuring alcohol dehydration (and activity in other catalytic reactions) in order to evaluate catalytic activity. Otherwise, a part of the surface remains covered by carbon dioxide and potentially other impurities).

Because dehydroxylation of the O_5Al^{VI}-OH site leaves a coordinatively unsaturated $Al^{V}O_5$ site, mobile Brønsted acid protons of bridging Al-OH-Al are required to form water from dehydroxylation (as discussed vide supra). Thus, we postulate that the -OH groups represented by the $\approx$3660–3680 cm^{-1} IR band belong to the different families of bridging, most likely, doubly bridging Al-OH-Al sites. The triply bridging OH groups likely manifest themselves as bands between 3600 and 3520 cm^{-1} (Figure 1a, Figure 2a). The intense band(s) between 3740–3720 cm^{-1} that remain upon surface dehydroxylation at high temperature (700 °C) under high vacuum on γ-alumina (Figure 1a, Figure 2b) and on other transition-aluminas (in particular, theta-alumina[22,29]), therefore, belong to O_3Al^{IV}-OH sites. These sites do not lose -OH group even at higher temperature due to unfavourability

of formation of $Al^{III}{}_1O_3$ sites, as noted previously by DFT. These tetrahedral O_3Al^{IV}-OH sites that survive high-temperature vacuum annealing without dehydroxylation, thus bear similarity with isolated tetrahedral silanol O_3Si^{IV}-OH of silica surfaces with OH stretches at $\approx 3740\ cm^{-1}$.[30]

In the study of Taoufik et al.,[31] experimental evidence from hetero- and homonuclear NMR spectra showed non-random distribution of surface sites on high surface area γ-alumina ($200\ m^2\,g^{-1}$). However, the authors attributed the band at $\approx 3770\ cm^{-1}$ to tetrahedral $O_3Al(IV)$-OH sites. The signal in the proton NMR spectra at $-\approx 0.2$ ppm was assigned to $O_3Al(IV)$-OH sites on the basis of amorphous low-nuclearity cluster models of Al-OH groups. We believe that the assignment of the $\approx 3770\ cm^{-1}$ band reported in ref. [31] needs to be re-evaluated. The amorphous cluster models used are far from realistic and do not provide accurate conclusions regarding specific assignments.[32] With our new findings, if one were to assume that the ≈ 3780–$3770\ cm^{-1}$ band belonged to the tetrahedral site with an -OH group, its dehydroxylation would result in a "bare" site (without the OH group). Based on the intensity of the ≈ 3780–$3770\ cm^{-1}$ band (which is significant), its dehydroxylation would result in significant amounts (on the order of at least 1% of total Al) of tri-coordinate Al sites: however, NMR shows no loss of such significant Al amounts and evolution of only 5-coordinate sites on the surface of alumina at the expense of the octahedral sites. Thus, it once again confirms our assignment that the ≈ 3780–$3770\ cm^{-1}$ sites belong to a family of octahedral O_5Al^{VI}-OH sites which form "bare" O_5Al^{V} sites upon thermal dehydroxylation.

After N_2 adsorption on the Al_P (penta-coordinate Al^{3+}) site, CO was dosed to observe the changes to the FTIR spectrum (Figure 4a).

The intensity of the N-N stretching vibrational feature of N_2 adsorbed on the $Al^{V}O_5$ site decreases concomitant with the development of a sharp band at 2240–2239 cm^{-1} (FWHM $\approx 13\ cm^{-1}$) of adsorbed CO. This indicates that CO selectively displaces N_2 on that site, forming a well-defined O_5Al^{VI}-CO

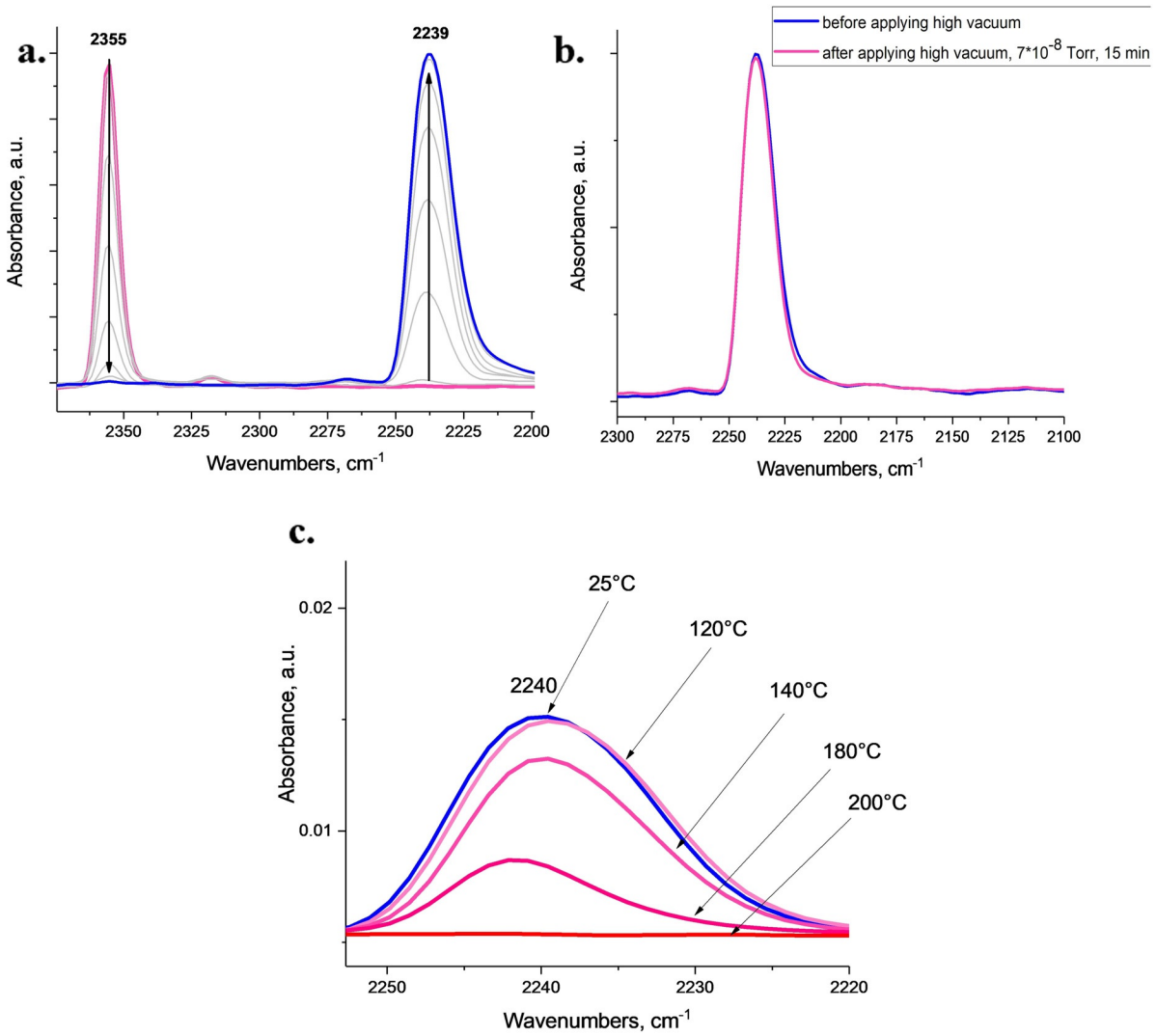

Figure 4. a) in situ FTIR during CO adsorption (equilibrium pressure ≈1 torr) on the 500 °C annealed alumina saturated with N_2 at 25 °C. b) Application of high vacuum on CO_{ads}/Al_2O_3, showing its high stability. c) Annealing of CO_{ads}/Al_2O_3 under vacuum from 25 to 200 °C.

carbonyl complex. The reaction is irreversible, and only high pressure (> 10 torr) of N_2 is required to reform a small portion of the initial IR signature of the dinitrogen complex (Figure S15). This Al carbonyl complex is exceptionally stable under both high vacuum and annealing (Figure 4b and c), up to 100 °C. Decomposition sets in above 130 °C and is completed at ≈200 °C (Figure 4c). In this instance, the CO stretch is upshifted by the ≈100 cm^{-1} compared to the gas phase CO. As such, it can be identified as a non-classical carbonyl metal complex.[33,34] No other solid material has CO bands vibrating at such high frequencies, exceeding even the previously described super electrophilic Pd^{II}, Pt^{II} and Ni^{II} cations on zeolites whose CO complexes exhibit a vibrational feature at/below ≈2220 cm^{-1}.[33,34] (N_2 adsorption and CO displacement experiments at 77 K followed by vacuum treatment of the CO complexes can be found in Figures S12,13.)

CO adsorption on alumina is typically characterized by a relatively wide feature with a maximum at ≈2230 cm^{-1}. No definitive assignments for this broad/wide signal have been provided. Herein, it is illustrated that the intensity of the 2240 cm^{-1} region of the wide signal depends on the extent of surface dehydroxylation. It is concluded that two components exist: the 2240 cm^{-1} (CO adsorbed strongly on penta-Al) and the 2225 cm^{-1} (CO adsorbed weaker on tetra-coordinate Al sites as seen in Figure S12, S13). The 2225 cm^{-1} component disappears completely upon evacuation even below 25 °C. The difference between the stability of the Al carbonyl complexes on AlO_4 and AlO_5 sites is likely related to the presence of the fifth O ligand trans to the CO ligand, uniquely stabilizing the first well-defined, thermally stable O_5-Al^{VI}-CO carbonyl complex.

Having shown the identity of the ≈3780–3770 cm^{-1} band as the O_5Al^{VI}-OH site on the reconstructed (110) surface as well as (depending on geometry) (100) surface, this group is shown to be basic and amphoteric. The amphotericity of this -OH group is proven by adsorbing Na^+ ions on the surface. The -OH intensity in this region dramatically decreases, confirming Na-O-Al linkage formation (Figure S14). Simultaneously, with the decrease of this band, activity in ethanol dehydration to ethylene drops precipitously (Figure S4,S5). Moreover, pyridine (basic molecule) also reacts with those sites with the formation of a pyridinium complex (not shown). Chupas et al. reported,[35] using pair-distribution-function methods and synchrotron XRD, that dehydroxylated γ-alumina surface contains Lewis acid sites capable of adsorbing monomethylamine CH_3NH_2 molecules: these Lewis sites were shown to be penta-coordinate sites, in excellent agreement with our findings.[35]

In previous studies the selective coordination of Pt and Ba ions to Al_P sites was shown.[23] Now we propose that the reaction between Al_p-OH and M-OH (where M is Pt, Na, or Ba) drives this interaction:

$$O_5Al(VI)\text{-}OH + M\text{-}OH \rightarrow O_5Al(VI)\text{-}O\text{-}M + H_2O. \quad (3)$$

Activity of the SBA-200 and rhombus-platelet samples for ethanol dehydration is shown in Figure S4 and S5. When the O_5Al^{VI}-OH groups at 3770 cm^{-1} are poisoned with Na ions with the formation of O_5Al^{VI}-O-Na units (Figure S14), the activity is significantly retarded (activity data are summarized in Figure S4,S5 for rhombus-platelet and SBA-200 samples with and without Na). Indeed, Datye and co-workers in their study on the ethanol dehydration activity of various alumina samples found that the most active transition aluminas for alcohol dehydration always possessed high relative fractions of the -OH band at ≈3770 cm^{-1}.[36] At the time, the precise identity of this band was not identified. Therefore, the culmination of the data in our study enables the unambiguous conclusion that ethanol dehydration largely takes place on the O_5Al(VI)-OH sites of the reconstructed (110) facets of the γ-Al_2O_3 surface for the typical rhombus-platelet alumina. Since this Al-OH group is basic, it activates weakly acidic ethanol resulting in the formation of Al-ethoxide. From O_5Al^{VI}-O-CH_2-CH_3, decomposition enables C_2H_4 to evolve, completing the catalytic cycle (Scheme 1).

Taking advantage of the state-of-the-art synthesis methods, we further prepared the rhombus-platelet, platelet and rod-like γ-alumina samples with similar surface areas ≈70 m^2g^{-1}: as we noted earlier, the rhombus-platelet sample lacks the macroscopically defined (100) facets. By varying the aspect ratio (i.e., elongating the crystals) we increased the surface area of the macroscopically defined (100) facets [which is maximized for the rod-like γ-alumina sample]. In

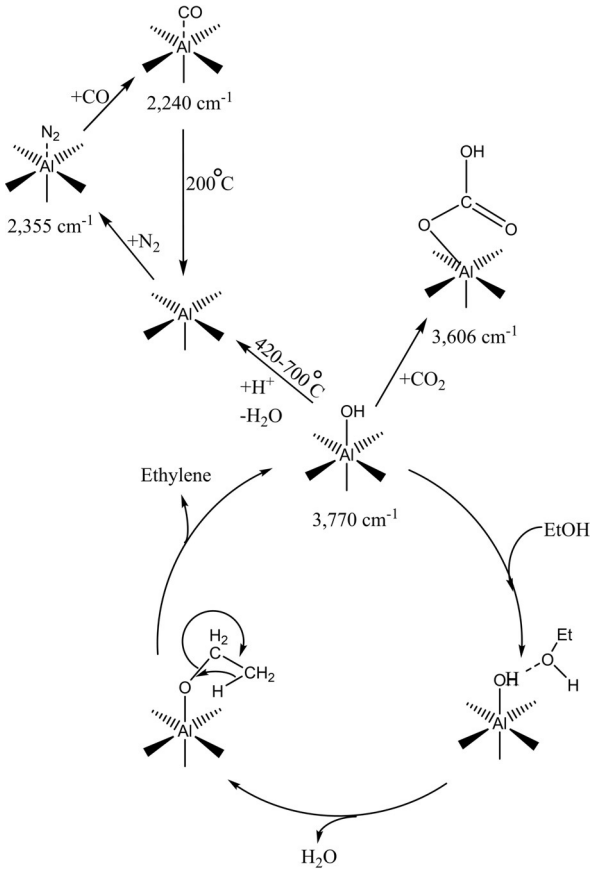

Scheme 1. Catalytic cycle for ethanol dehydration as well as interactions with probe molecules described in our study for the parent O_5Al(VI)-OH site as well as dehydroxylated Al^VO_5 sites on the surface of γ-alumina.

accordance with our suggestions, the rod-like sample with the maximized amount of (100) facets possessed the highest relative amount of ≈3780–3770 cm^{-1} (octahedral O_5Al^{IV}-OH group) and ≈3660 cm^{-1} (doubly bridging Al-OH-Al bands) (Figure S16). It also possessed the highest activity in both dissociative ethanol TPD and catalytic ethanol dehydration studies (Figure S17,S18) with activity linearly increasing with the relative increase of the macroscopically defined (100) facet, in excellent agreement with our conclusions. Furthermore, our new findings can now explain how certain alumina samples lacking the macroscopically defined (100) facets still possess high reactivity in alcohol dehydration. This, of course, occurs due to breaking down of macroscopic (110) facet into (100) and (111) nano-facets due to their higher thermodynamic stability.

Conclusion

Although γ-alumina is one of the oldest and largest-scale commercial catalytic materials, the precise identification of its catalytically active sites has remained elusive. With the aid of state-of-the-art FTIR, high-field solid state NMR, and HRTEM techniques, clarification of the nature of the active sites on the surface of γ-alumina for ethanol dehydration (as well as anchoring of organometallic fragments and CO/N_2 activation) is proposed, providing the atomic-scale guidelines for the design of more active materials in the future.

Acknowledgements

The research at PNNL was supported by the U.S. Department of Energy (DOE), Office of Science, Basic Energy Sciences, Chemical Sciences, Geosciences and Biosciences Division at Pacific Northwest National Laboratory (PNNL). (DE-AC05-76RL01830, FWP 47319). Experiments were conducted in the Environmental Molecular Sciences Laboratory (EMSL), a national scientific user facility sponsored by the Department of Energy's Office of Biological and Environmental Research at Pacific Northwest National Laboratory (PNNL). PNNL is a multi-program national laboratory operated for the DOE by Battelle Memorial Institute under Contract DE-AC05-76RL01830.

Conflict of interest

The authors declare no conflict of interest.

Keywords: alumina · electron microscopy · ethanol dehydration · heterogeneous catalysis · solid-state NMR spectroscopy

[1] W. Ipatiew, *J. Prakt. Chem.* **1903**, *67*, 420.
[2] M. W. Steward, H. W. Clark, D. P. Coffey, L. Luo, A. E. Schweizer (Dow Global Technologies), U.S. Patent 9242919, **2016**.
[3] A. Zecchina, S. Califano, *The Development of Catalysis: A History of Key Processes and Personas in Catalytic Technology*, Wiley, Hoboken, **2017**.
[4] A. V. Grosse, V. N. Ipatieff, *Ind. Eng. Chem.* **1940**, *32*, 268–272.
[5] M. Boudart, *Catalysis by Supported Metals*, *Vol. 20* (Ed.: W. G. Frankenberg), Academic Press, New York, **1969**, chap. XX.
[6] K. H. Buchel, H.-H. Moretto, P. Woditsch, *Industrial Inorganic Chemistry*, 2nd ed., Wiley-VCH, Weinheim, **2000**.
[7] "Catalysis from Art to Science": W. M. H. Sachtler in *Surface Chemistry and Catalysis. Fundamental and Applied Catalysis* (Eds.: A. F. Carley, P. R. Davies, G. J. Hutchings, M. S. Spencer), Springer, Boston, **2002**.
[8] L. Kovarik, M. Bowden, A. Genc, J. Szanyi, C. H. F. Peden, J. H. Kwak, *J. Phys. Chem. C* **2014**, *118*, 18051–18058.
[9] L. Kovarik, M. Bowden, D. Shi, N. M. Washton, A. Andersen, J. Z. Hu, J. Lee, J. Szanyi, J. H. Kwak, C. H. F. Peden, *Chem. Mater.* **2015**, *27*, 7042–7049.
[10] L. Kovarik, A. Genc, C. Wang, A. Qiu, C. H. Peden, J. Szanyi, J. H. Kwak, *J. Phys. Chem. C* **2013**, *117*, 179–186.
[11] L. Kovarik, M. Bowden, D. Shi, J. Szanyi, C. H. F. Peden, *J. Phys. Chem. C* **2019**, *123*, 9454–9460.
[12] R. Prins, *Angew. Chem. Int. Ed.* **2019**, *58*, 15548–15552; *Angew. Chem.* **2019**, *131*, 15694–15698.
[13] R. Prins, *J. Catal.* **2020**, *392*, 336–346.
[14] M. Digne, P. Sautet, P. Raybaud, P. Euzen, H. Toulhoat, *J. Catal.* **2004**, *226*, 54–68.
[15] R. Wischert, C. Copéret, F. Delbecq, P. Sautet, *Chem. Commun.* **2011**, *47*, 4890–4892.
[16] R. Wischert, P. Laurent, C. Copéret, F. Delbecq, P. Sautet, *J. Am. Chem. Soc.* **2012**, *134*, 14430–14449.
[17] R. Wischert, P. Florian, C. Copéret, D. Massiot, P. Sautet, *J. Phys. Chem. C* **2014**, *118*, 15292–15299.
[18] R. Wischert, C. Copéret, F. Delbecq, P. Sautet, *Angew. Chem. Int. Ed.* **2011**, *50*, 3202–3205; *Angew. Chem.* **2011**, *123*, 3260–3263.
[19] A. Salameh, J. Joubert, A. Baudouin, W. Lukens, F. Delbecq, P. Sautet, J. M. Basset, C. Copéret, *Angew. Chem. Int. Ed.* **2007**, *46*, 3870–3873; *Angew. Chem.* **2007**, *119*, 3944–3947.
[20] M. Valla, R. Wischert, A. Comas-Vives, M. P. Conley, R. Verel, C. Copéret, P. Sautet, *J. Am. Chem. Soc.* **2016**, *138*, 6774–6785.
[21] H. Knözinger, P. Ratnasamy, *Catal. Rev. Sci. Eng.* **1978**, *17*, 31–70.
[22] G. Busca, *Catal. Today* **2014**, *226*, 2.
[23] J. H. Kwak, J. Hu, D. Mei, C.-W. Yi, D. H. Kim, C. H. F. Peden, L. F. Allard, J. Szanyi, *Science* **2009**, *325*, 1670–1673.
[24] J. Lee, E. J. Jang, H. Y. Jeong, J. H. Kwak, *Appl. Catal. A* **2018**, *556*, 121.
[25] J. H. Kwak, D. Mei, C. H. F. Peden, R. Rousseau, J. Szanyi, *Catal. Lett.* **2011**, *141*, 649–655.
[26] S. A. Zubkov, V. Y. Borovkov, S. G. Gagarin, V. B. Kazanskii, *Chem. Phys. Lett.* **1984**, *107*, 337.
[27] N. R. Jaegers, J. K. Lai, Y. He, E. Walter, D. A. Dixon, M. Vasiliu, Y. Chen, C. M. Wang, M. Y. Hu, K. T. Mueller, I. E. Wachs, Y. Wang, J. Z. Hu, *Angew. Chem. Int. Ed.* **2019**, *58*, 12609–12616; *Angew. Chem.* **2019**, *131*, 12739–12746.
[28] N. R. Jaegers, K. T. Mueller, Y. Wang, J. Z. Hu, *Acc. Chem. Res.* **2020**, *53*, 611—619.
[29] L. Kovarik, M. Bowden, J. Szanyi, *J. Catal.* **2021**, *393*, 357–368.
[30] S. P. Zhdanov, L. S. Kosheleva, T. I. Titova, *Langmuir* **1987**, *3*, 960–967.
[31] M. Taoufik, et al., *Chem. Eur. J.* **2014**, *20*, 4038–4046.
[32] L. Kovarik, M. Bowden, A. Andersen, N. R. Jaegers, N. Washton, J. Szanyi, *Angew. Chem. Int. Ed.* **2020**, *59*, 21719–21727; *Angew. Chem.* **2020**, *132*, 21903–21911.
[33] K. Khivantsev, N. R. Jaegers, I. Z. Koleva, H. A. Aleksandrov, L. Kovarik, M. Engelhard, F. Gao, Y. Wang, G. N. Vayssilov, J. Szanyi, *J. Phys. Chem. C* **2020**, *124*, 309–321.

[34] N. R. Jaegers, K. Khivantsev, L. Kovarik, D. Klas, J. Z. Hu, Y. Wang, J. Szanyi, *Catal. Sci. Technol.* **2019**, *9*, 6570 – 6576.
[35] P. J. Chupas, K. W. Chapman, G. J. Halder, *J. Am. Chem. Soc.* **2011**, *133*, 8522 – 8524.
[36] S. Srinivasanab, C. R. Narayanan, A. K. Datye, *Appl. Catal. A* **1995**, *132*, 289 – 308.

Manuscript received: February 9, 2021
Revised manuscript received: April 9, 2021
Accepted manuscript online: April 26, 2021
Version of record online: June 29, 2021

